The Lateral Distribution Function of Coherent Radio Emission from Extensive Air Showers; Determining the Chemical Composition of Cosmic Rays

Krijn D. de Vries, Ad M. van den Berg, Olaf Scholten, Klaus Werner

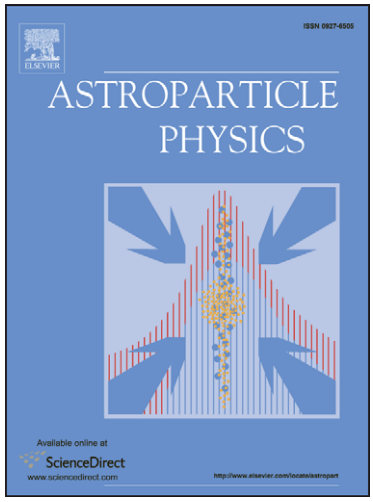

The Lateral Distribution Function of Coherent Radio Emission from Extensive Air Showers; Determining the Chemical Composition of Cosmic Rays

Krijn D. de Vries, Ad M. van den Berg, Olaf Scholten, Klaus Werner

PII: S0927-6505(10)00143-X
DOI: 10.1016/j.astropartphys.2010.08.003
Reference: ASTPHY 1514

To appear in: *Astroparticle Physics*

Received Date: 21 January 2010
Revised Date: 4 August 2010
Accepted Date: 4 August 2010

Please cite this article as: K.D. de Vries, A.M. van den Berg, O. Scholten, K. Werner, The Lateral Distribution Function of Coherent Radio Emission from Extensive Air Showers; Determining the Chemical Composition of Cosmic Rays, *Astroparticle Physics* (2010), doi: 10.1016/j.astropartphys.2010.08.003

The Lateral Distribution Function of Coherent Radio Emission from Extensive Air Showers; Determining the Chemical Composition of Cosmic Rays

Krijn D. de Vries[a], Ad M. van den Berg[a], Olaf Scholten[a], and Klaus Werner[b]

[a] *Kernfysisch Versneller Instituut, University of Groningen, 9747 AA, Groningen, The Netherlands*
[b] *SUBATECH, University of Nantes – IN2P3/CNRS– EMN, Nantes, France*

Abstract

The lateral distribution function (LDF) for coherent electromagnetic radiation from air showers initiated by ultra-high-energy cosmic rays is calculated using a macroscopic description. A new expression is derived to calculate the coherent radio pulse at small distances from the observer. It is shown that for small distances to the shower axis the shape of the electric pulse is determined by the 'pancake' function, describing the longitudinal distribution of charged particles within the shower front, while for large distances the pulse is determined by the shower profile. This reflects in a different scaling of the LDF at small and at large distances. As a first application we calculate the LDF for proton- and iron-induced showers and we show that this offers a very sensitive measure to discriminate between these two. We show that due to interference between the geo-magnetic and the charge-excess contributions the intensity pattern of the radiation is not circular symmetric.

Key words: Radio detection, Air showers, Cosmic rays, Geo-synchrotron, Geo-magnetic, Coherent radio emission, Mass determination

1. Introduction

In recent years much progress has been made modeling electric pulses initiated by extensive air showers (EAS) [1, 2, 3]. One of the reasons for this progress are the results from the LOPES [4, 5] and CODALEMA [6, 7] experiments. Both experiments indicate that the dominant emission mechanism is due to induction effects from the Earth's magnetic field which exerts a Lorentz force on the charged particles in the shower. The emission process can be described in a microscopic model where the individual electrons and positrons move on cyclotron orbits [1, 8, 9, 10]. The importance of coherent radio emission was already noted in earlier research on radio emission from air showers [11, 12, 13, 14]. Recently, this approach has received renewed attention with the realistic calculations in the Macroscopic Geo-Magnetic Radiation (MGMR) model as presented in Ref. [2].

The experimental results have triggered plans for an extensive array of radio detectors at the Pierre Auger Observatory [15, 16, 17]. A clear theoretical understanding of the pulse shape and its dependence on the distance from the shower axis is therefore of importance. In the present paper we derive a new expression for the electromagnetic pulse that is more appropriate for observer positions that are closer to the shower axis while the expression derived in Ref. [2] is appropriate for large distances. This allows us to address quantitatively the differences in the structure of the electromagnetic pulse emitted by the EAS at large and small distances. It was already noticed in an earlier study [2] that in a macroscopic calculation the structure of the electromagnetic pulse at small distances is strongly affected by the distribution of the particles in the shower front (the pancake). In Ref. [18] the importance of length scales was emphasized in the understanding of macroscopic geo-magnetic radiation from the EAS indicating that the physics at short distances differs from that at large distances.

In Ref. [1] it is argued that in the synchrotron-emission model REAS2, the lateral distribution function (LDF) can be used to disentangle the chemical composition of cosmic rays. As shown in Ref. [19] the predictions of the macroscopic model and the synchrotron-emission models such as used in Refs. [1, 20, 21] differ greatly. In particular the latter models predict a unipolar pulse which contradicts the fact that the intensity of the emitted radiation should vanish at the longest wavelength [18], a condition that is satisfied by the bi-polar pulse in the MGMR model. Recently [22, 23], it has been shown that this is due to the omission of the bremsstrahlung contributions at the beginning and the end of the particle trajectories in the synchrotron-emission models. This effect is now included in an updated version of the geo-synchrotron code REAS3 [22]. Therefore, we will investigate here, as an application of the new calculation scheme for the MGMR model, the differences in the LDF for iron- and proton-

Email address: scholten@kvi.nl (Olaf Scholten)

induced showers.

In Section 2 a quick overview of the MGMR model is given. For completeness we will shortly review the derivation of the expression for the electric field. As the next step we concentrate on the short distance scales in Section 3 where a new expression is derived for the electric field at small impact parameters. For simplicity, we will limit ourselves to vertical incoming air showers. The geometry considered is an incoming shower with velocity $\vec{\beta} = -\beta\hat{z}$, an observer placed at a distance $\vec{d} = d\hat{x}$ from the shower axis with a magnetic field $\vec{B} = B\hat{y}$ perpendicular to the air shower. The realistic case will be treated in a forthcoming publication. As a first application of the new calculation scheme it is shown in Section 4 that the LDF depends on the orientation of the observer with respect to the shower axis. This angular dependence is due to interference of the leading magnetic contribution with secondary contributions. Of these secondary contributions, the one which is generated by charge excess in the shower is the most important. As a second application the influence of the chemical composition of the cosmic ray on the LDF is discussed in Sections 5 and 6.

2. The model

When an ultra-high energy cosmic ray collides in the atmosphere, a cascade of secondary particles is created, moving towards the Earth with a velocity close to that of the speed of light. This can be visualized by a 'pancake' of particles. The basic picture in the MGMR model [2] is that the charged particles in the pancake, mostly electrons and positrons, will be deflected in the Earth's magnetic field causing the flow of a macroscopic electric current. The strength of this electric current is time dependent and thus radiates. We will temporarily make the assumption that there is an equal amount of electrons and positrons in the shower; in a later section the effects of charge excess will be discussed.

The total amount of electrons and positrons traveling in the shower front can be described as a function of height $z = -c\beta_s t' + h$, where t' is the shower time (negative) and the front of the shower hits the Earth at $t' = 0$. This implies that the front of the shower is located at a height of $z = -c\beta_s t'$ with the particles lagging behind at a distance within the pancake following a distribution $f_p(h)$. The distribution of particles is given as

$$N(z, t') = N_e f_t(t')\, f_p(h) \tag{1}$$

where $f_t(t')$ is the normalized shower profile, and the total number of particles at the shower maximum equals $N_e = 6 \times (E_p/10^{10}\text{eV})$ defined by the maximum number of particles for a 10^{19} eV shower [24].

The longitudinal profile $N_e f_t(t')$ is parametrized [25] as a function of the penetration depth X in units of g cm^{-2},

$$N_e f_t(t) = N_e e^{(X - X_{max} - 1.5X\ln s)/X_0}\ , \tag{2}$$

The penetration depth is written as a function of height as $X(z) = (\rho(0)/C)e^{-Cz_s}$. Using $\rho(0) \approx 1168$ g m^{-3}, and $X(0) \approx 1000$ g cm^{-2} gives $C = 1.168 \cdot 10^{-4}$ m^{-1}. The parameter X_{max} is taken to reproduce the shower maximum from simulations [24], $X_{max} = (840{+}70\log_{10}(E_p/10^{20}\text{ eV}))$ g cm^{-2}. The shower age $s(X)$ can be parameterized as [25],

$$s(X) = \frac{3X/X_0}{X/X_0 + 2X_{max}/X_0}, \tag{3}$$

where $X_0 = 36.7$ g cm^{-2} is the radiation length of electrons in air.

For the pancake thickness a parametrization can be made using measured arrival time distributions. This can be fitted using a Γ-probability distribution function (Γ-pdf) [25, 26],

$$f_p(h) = h^\beta e^{-2h/L} \times (4/L^2), \tag{4}$$

where $\beta = 1$ and $L = 3.9$ m have been used, see Section 5.

The electrons and positrons will be deflected in the Earth's magnetic field which macroscopically induces a net current in the $\hat{x}$ direction given by,

$$j^x(x, y, z, t') = \langle v_d q\rangle\, e\, N(z, t')\delta(x)\delta(y)\ , \tag{5}$$

where q is the sign of the electric charge e. We disregard the lateral distribution of the charged particles and fix the position of the charged particles at the shower axis. The drift velocity, $\langle v_d q\rangle$, depends rather strongly on the model assumptions made [3] and we adopt a value of $\langle v_d q\rangle = 0.025\ c$.

The vector potential is given by the Liénard-Wiechert fields [27] in terms of the current density, j^x,

$$A^x(t, \vec{d}) = J_0 \int_{\mathcal{D}} f_t(t_r) f(h)\ dh\ , \tag{6}$$

where $J_0 = \langle v_d q\rangle N_e e/\left[4\pi\varepsilon_0 c\right]$, d is the distance from the observer to the shower axis, and where the retarded distance can be rewritten as

$$\mathcal{D} = \sqrt{(-c\beta_s t + h)^2 + (1 - n^2\beta_s^2)d^2}\ . \tag{7}$$

The retarded time is defined by $c(t - t_r)/n = R$, where $R = \sqrt{(z^2 + d^2)}$, n is the index of refraction of air and can be expressed as [2, 3],

$$ct_r = \frac{ct - n^2\beta_s h - n\mathcal{D}}{(1 - n^2\beta_s^2)}\ . \tag{8}$$

At a large distance from the shower axis the point-like approximation [2, 19] is valid in which the pancake thickness is set to zero, $f_p(h) = \delta(h)$. In this limit a simple analytical expression for the electric field can be derived [2],

$$E_x(t, \vec{d}) \approx J_0 \frac{c^2 t_r^2 4}{dt_r}\left[t_r f_t(t_r)\right]\ , \tag{9}$$

with $ct_r \approx -d^2/2ct$. In general this approximation is valid at typical distances above $d = 500$ m since the typical time window for the pulse lies between 10^{-8} and 10^{-7} s. From Eq. (9) we see that the electric field scales as d^{-4} and that the integral over time vanishes (i.e. zero response at zero frequency) when the shower profile vanishes at the Earth's surface.

3. Radial dependence of the pulse strength

For the shape of the pulse it is very important to understand the interplay between the different length scales [18]. While at large distances from the shower the important length scale is related to a projection of the shower profile along the line of sight of the observer, we will show in this section that for small distances the pancake thickness parameter, L, is important. To describe the electric field for small impact parameters we encounter the problem that the integral in Eq. (6) becomes numerically unstable. We therefore first derive a new equation for the pulse which is particularly suited at small distances from the core.

For an observer placed close to the shower axis it is more transparent to change variables in Eq. (6) and integrate over the retarded shower time at which the signal is emitted since the signal moves with the same velocity as the shower. The vector potential can thus be written as,

$$\begin{aligned} A^x(t,\vec{d}) &= J_0 \int_{t_r^-(t)}^{t_r^+(t)} dt_r \frac{\partial h}{\partial (ct_r)} \frac{f_t(t_r)}{\mathcal{D}} f_p(h) \\ &= -J_0 \int_{t_r^-(t)}^{t_r^+(t)} dt_r \frac{f_t(t_r)}{z} f_p(h) \; . \end{aligned} \tag{10}$$

The retarded time t_r is related to the observing time t and the distance from the shower front h by Eq. (8) which can be rewritten in the limit $n = 1$ and $\beta_s = 1$ as

$$ct_r = \frac{c^2t^2 - d^2 - h^2}{2(ct + h)} \; , \tag{11}$$

The Jacobian in this case is non-zero due to the fact that at a fixed observer time t, the received signal is emitted at different shower times, depending on the emission point within the pancake. Hence, $t_r^- = -\infty$ and $t_r^+ = t_r(t, h = 0)$ for a fixed observer time t. The Jacobian can now be derived from Eq. (11),

$$\frac{\partial h}{\partial (ct_r)} = \frac{\mathcal{D}}{ct_r - h} \tag{12}$$

The electric field now becomes

$$\begin{aligned} E^x(t,\vec{d}) &= -J_0 \int_{t_r^-(t)}^{t_r^+(t)} dt_r f_t(t_r) \frac{d}{dt} \left(\frac{f_p(h)}{z} \right) \\ &= -J_0 \int_{t_r^-(t)}^{t_r^+(t)} dt_r f_t(t_r) \left(\frac{d}{dt} + \frac{d}{dt_r} \right) \left(\frac{f_p(h)}{z} \right) \\ &- J_0 \int_{t_r^-(t)}^{t_r^+(t)} dt_r \frac{df_t(t_r)}{dt_r} \frac{f_p(h)}{z} \\ &- \frac{f_t(t_r) f_p(h)}{z} \Big|_{t_r^-(t)}^{t_r^+(t)} \end{aligned} \tag{13}$$

Now using

$$\left(\frac{d}{dt} + \frac{d}{dt_r} \right) \left(\frac{f_p(h)}{z} \right) = \frac{\beta}{z} \frac{df_p(h)}{dh} \tag{14}$$

we can write

$$\begin{aligned} E^x(t,\vec{d}) &= -J_0 \int_{t_r^-(t)}^{t_r^+(t)} dt_r f_t(t_r) \frac{\beta}{z} \frac{df_p(h)}{dh} \\ &- J_0 \int_{t_r^-(t)}^{t_r^+(t)} dt_r \frac{df_t(t_r)}{dt_r} \frac{f_p(h)}{z} \end{aligned} \tag{15}$$

where the terms coming from the derivative working on the integration limits and the partial integration vanish due to the fact that the f_p vanishes at the limits, and where t, t_r and h are related by Eq. (8). For very small impact parameters the second term on the right-hand side in Eq. (15) becomes an integral over the time derivative of the shower profile and vanishes at the given limits. This happens since the signal travels along with the shower and thus h becomes approximately independent of t_r. Hence the main contribution to the electric field for very small impact parameters comes from the first term on the right-hand side of equation Eq. (15).

When the shower profile is finite at the surface of the Earth, $z = 0$, the terms in Eq. (15) suffer from a $1/z$ divergence. To regularize this divergence we introduce an exponential suppression term in the shower profile function,

$$F_t(t_r) = f_t(t_r) - f_t(0) e^{-z/a}, \tag{16}$$

where a is the cut-off distance. The divergence in Eq. (15) is now eliminated since the shower profile function vanishes linearly for $z = 0$. The electric field for different values of a is given in Fig. 1 where the simulations are done for a vertical incoming shower with a primary energy of $E_p = 10^{18}$ eV. The calculations show that at a distance of $d = 50$ m even a value as large as $a = 1000$ m hardly affects the pulse. At a distance of only $d = 10$ m a value of $a = 100$ m gives already a stable result. It has been verified that this result hardly depends on the altitude of the observer or energy of the cosmic ray, and can also be used for more energetic showers where the shower maximum is close to the Earth's surface. This is due to the fact that the maximum of the observed electric field is emitted well before the shower is fully developed. We note here that, therefore the observation of radio signals from air showers are particularly suited to study the early stages of the shower developement. Interesting to notice is that the signal at a distance of only 50 m from the core is hardly affected by the shower properties at a height below 1 km.

Another interesting aspect of Fig. 1 is that the pulse-shape does not vary strongly with distance. At large distances where Eq. (9) applies one expects a variation like d^2 in pulse length. Instead one finds that the zero-crossing

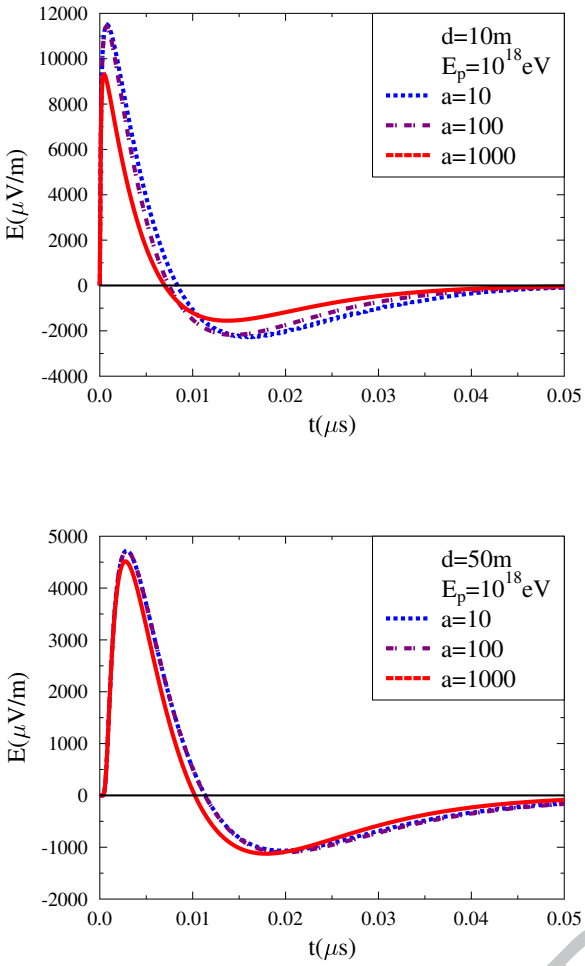

Figure 1: The unfiltered electric field for different values of the cut-off parameter $a = 10$, $a = 100$, and $a = 1000$, at a distance $d = 10$ m (top) and $d = 50$ m (bottom) from the shower axis. The pancake thickness parameter is taken as $L = 3.9$; see Section 5.

of the pulse changes from 9 to 11 ns while the distance changes by a factor 5 from $d = 10$ to 50 m. This time scale corresponds to a length scale of about 3 m which is determined by the pancake thickness as supported by test calculations.

The dependence of the calculated pulse height on d is shown in Fig. 2. Based on Eq. (9) one would expect the pulse strength to be proportional to d^{-4} as given by the black line in the figure. Only at very large distances this dependence is seen.

In Fig. 3 the power P above 25 MHz divided by that at a distance of $d = 50$ m is plotted as a function of d. This quantity can easily be compared to actual measurements since the power is not affected by dispersion of the signal contrary to the pulse height and it corresponds to a semi-realistic filtering of the pulse. It is clearly seen that

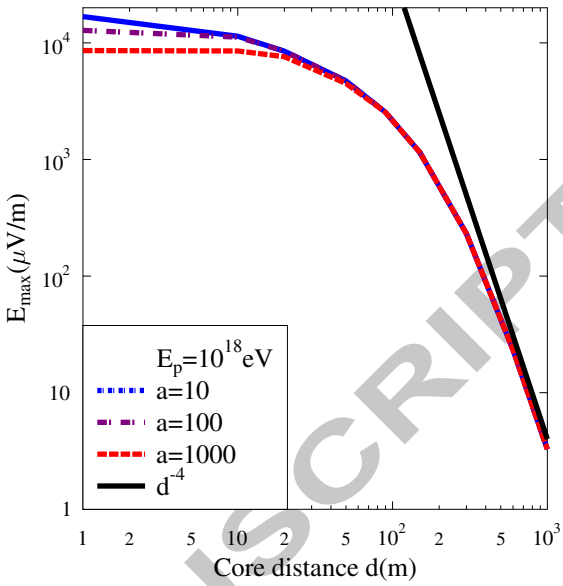

Figure 2: Lateral distribution function for the pulse height as function of distance on double logarithmic scale for different values of the cut-off parameter a.

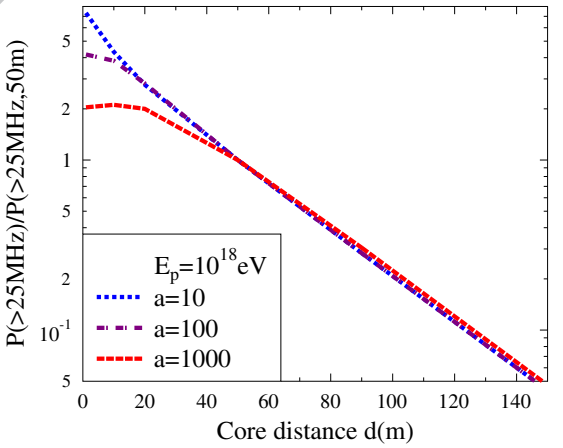

Figure 3: Lateral distribution function for the received power at frequencies above 25 MHz divided by that at a distance of $d = 50$ m.

for small distances a smaller value of a should be used to reach a convergent result. The LDF for the power shows a distinct exponential structure for distances beyond 5 m from the core where the power drops by one order of magnitude over a distance of close to 70 m.

For observer distances approaching $d = 0$ m the pulse height tends to diverge. Since, for $n = 1$, the signal travels

along with the shower with the same speed, an observer placed at the impact point of the shower will see the equivalent of a divergent Cherenkov peak. The precise structure of the pulse at very short distances will thus strongly depend on the index of refraction [3]. In addition one expects that at close proximity to the core the electric field is influenced by the lateral extent of the electrons in the shower since the particle density is strongly peaked near the shower axis. In a forthcoming publication we will look into this effect in more detail.

4. Interference

The main secondary contribution, which is important for the present discussion, is due to the charge excess in the shower [2, 3] which is due to knock out from ambient air molecules. The coherent emission from the charge excess in cosmic-ray induced showers was first discussed by Askaryan [28], where it is due to the creation and annihilation of energetic electrons. Even though the Askaryan effect is often associated with Cherenkov radiation, it also applies to the case in which the index of refraction is close to unity [29].

Macroscopically the charge-excess contribution can be described using a net negative charge moving with the speed of light toward the surface of the Earth. The contribution to the vector potential is now given by,

$$A^0_{Cx} = \frac{eN_e}{4\pi\epsilon_0} C_x \int_0^\infty dh \frac{f_t(t_r) f(h)}{\mathcal{D}} - \frac{e}{4\pi\epsilon_0} \int_{-\infty}^{t'} \left(\int_0^\infty dh \frac{df_t(t')}{dt'} \frac{f(h)}{R} \right) dt' \quad (17)$$

$$A^z_{Cx} = \frac{eN_e}{4\pi\epsilon_0} C_x \int_0^\infty dh \frac{-\beta f_t(t_r) f(h)}{\mathcal{D}}. \quad (18)$$

The electric field is now obtained by,

$$E^{Cx}_x(t) = \frac{-\partial A^0_{Cx}}{\partial x} = \frac{C_x e N_e}{4\pi\epsilon_0} \int_0^\infty dh \frac{x}{\mathcal{D}^2} \frac{z}{R} \dot{f}_t(t_r) f(h) \quad (19)$$

$$E^{Cy}_y(t) = \frac{-\partial A^0_{Cx}}{\partial y} = \frac{C_x e N_e}{4\pi\epsilon_0} \int_0^\infty dh \frac{y}{\mathcal{D}^2} \frac{z}{R} \dot{f}_t(t_r) f(h) \quad (20)$$

$$E^{Cx}_z(t) = \frac{-\partial A^0_{Cx}}{\partial z} - \frac{\partial A^z_{Cx}}{\partial ct} = \frac{C_x e N_e}{4\pi\epsilon_0} \int_0^\infty dh \frac{d}{\mathcal{D}^2} \frac{d}{R} \dot{f}_t(t_r) f(h) \quad (21)$$

where $C_x = 0.23$ is the approximate fraction of charge excess with respect to the total number of electrons and positrons in the shower as predicted by the Monte-Carlo simulations described in Section 5.

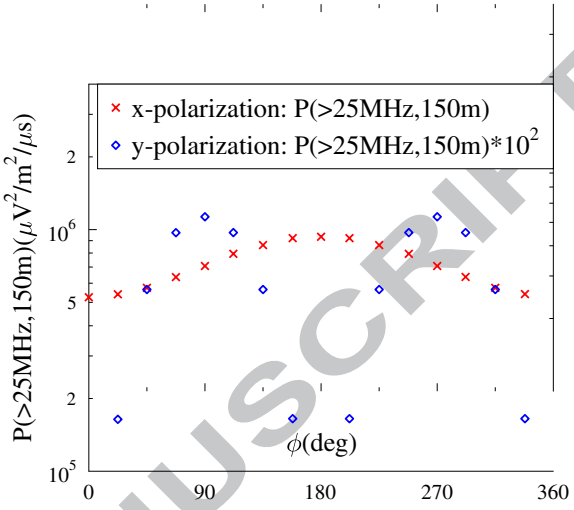

Figure 4: The strength of the signal for two different polarization directions is plotted as a function of the orientation of the observer with respect to the shower. The y-polarization has been multiplied by a factor 100 to put it on a similar scale. The magnetic field is chosen pointing to the North, while $\phi = 90°$ ($\phi = 180°$) corresponds to the observer at the East (North) side of the shower.

The interference of the geo-magnetic and the charge-excess contribution will be important for the observed pulse. For this interference the polarization of the two contributions should be considered. For a vertical shower ($\hat{z}$-direction) in a horizontal magnetic field ($\hat{y}$-direction) the electric pulse generated by the induced electric current is polarized in the $\hat{x}$-direction independent of the orientation of the observer with respect to the shower axis. The radiation due to charge excess is polarized radially. Depending on the position of the observer the two contributions may interfere destructively (observer on the negative x-axis, $y = 0$), constructively (observer on the positive x-axis, $y = 0$), or be orthogonal (observer anywhere on the y-axis). This effect can be seen clearly in Fig. 4 where the dependence of the signal strength in the $\hat{x}$-, and $\hat{y}$-direction is plotted as function of the orientation of the observer.

In Fig. 5 the LDF is shown separately for geo-magnetic and charge-excess radiation showing that while the two contributions differ by a factor 5 near the shower core, their magnitudes are about equal at a distance of 500 m. Depending on the orientation (azimuth) of the observer with respect to the shower the two contributions will interfere constructively or destructively. Since the charge-excess and the geo-magnetic contribution depend in a different way on the shower profile their LDF's differ. This gives rise to the interesting observation that for an ob-

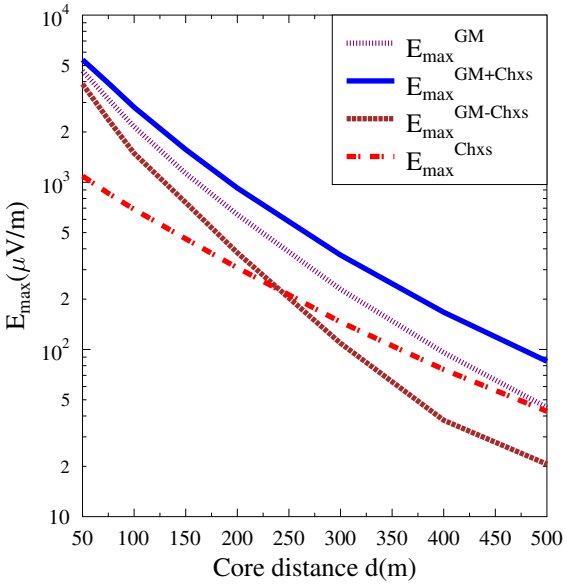

Figure 5: The behaviour of the LDF as a consequence of different types of interference between geo-magnetic radiation and charge excess radiation.

server at one side of the shower the charge-excess and the geo-magnetic contributions may interfere destructively resulting in a LDF that falls off rather steeply close to the core and flattens after the point of maximal destructive interference where even a local minimum could occur. For an observer positioned at the other side of the same shower the two contributions add constructively resulting in a relatively smooth LDF. In the perpendicular direction the two contributions will not interfere as their polarizations are orthogonal. The distance where a local minimum could occur and the LDF starts to flatten will depend on the relative magnitude of the charge-excess and the geo-magnetic contribution where the latter depends strongly on the angle of the shower with the magnetic field. It follows that one should be extremely careful in determining the LDF [30] since it is expected to depend on the orientation of the observer to the shower.

5. Hybrid approach

In the previous sections, all simulations were done using the basic MGMR model. The particle distributions in these simulations were parametrized using the analytical formula given in Section 2. In the current section we will discuss the hybrid approach to the MGMR model. Within this approach the important macroscopic properties describing the electric field, such as the pancake thickness and the shower profile, are obtained from Monte-Carlo simulations.

These simulations are done using the cascade mode of the CONEX shower simulation program [31, 32]. This code has been modified to include the deviation of charged particles in the Earth's magnetic field, which is discussed in detail in Appendix B of Ref. [3]. Furthermore an analysis tool has been written, giving a histogrammed output of the full three-dimensional and timing information of the currents and particle distributions within a user-defined region of the shower front which in the simplest case becomes an average of all particles over the complete shower front. Several examples for such distributions, smoothed by fitting procedures, can be found in Ref. [3], more details will be discussed in a future publication. The complete shower-simulation package including analysis tools is called CONEX-MC-GEO.

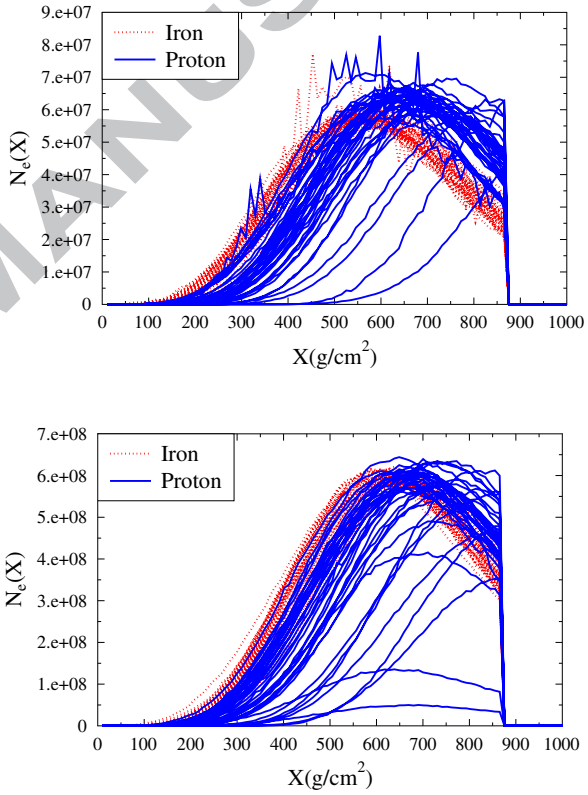

Figure 6: Total number of electrons and positrons as function of shower depth for 40 proton (blue curves) and 40 iron (red curves) initiated showers at energies $E = 10^{17}$ eV (top) and $E = 10^{18}$ eV (bottom).

As a first example the histogrammed output obtained by CONEX-MC-GEO, which will be used in Section 6 to study the differences of the LDF for a proton- and an iron-primary particle, will be discussed. The simulations are done for 40 proton- and 40 iron-induced showers to extract the longitudinal shower profiles and the pancake thicknesses at energies of 10^{17} and 10^{18} eV.

The obtained shower profiles are shown in Fig. 6. As is expected the shower-to-shower fluctuations are rather

large for proton- and small for iron-induced showers. It should be noted that the intrinsic fluctuations for a few showers become large. This is partially due to thinning effects. The X_{max} is larger for proton than for iron. The shower profile drops to zero at around 870 g cm^{-2} where the shower hits the surface of the Earth according to the conditions at the site of the Pierre Auger Observatory.

In the previous section the importance of the charge-excess contribution and its impact on the LDF is shown. To make this more quantitative the fraction of excess electrons is plotted in Fig. 7 for Monte-Carlo simulations of 40 proton- and 40 iron-induced showers at an energy of 10^{17} eV. An analysis for 10^{18} eV showers gives similar results. The charge excess is slightly increasing with increasing shower depth. Near the shower maximum the charge excess is close to 23% of the total number of electrons and positrons which is the value we have assumed in all our calculations described in Section 4. The charge-excess contribution scales linearly with the charge-excess fraction. The shower-to-shower fluctuations thus have a relatively small effect. The other important parameter for the radio-

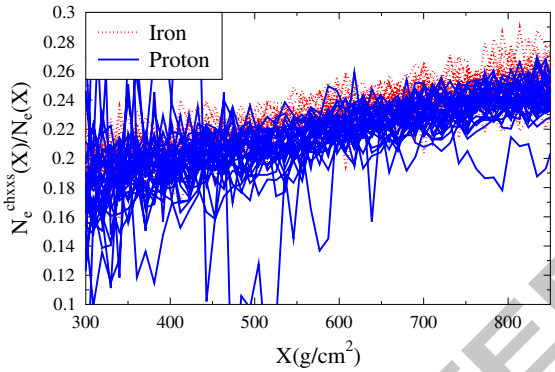

Figure 7: The fraction of charge-excess electrons with respect to the total number of electrons and positrons as a function of shower depth for 40 proton and 40 iron induced showers at an energy of 10^{17} eV.

emission calculations is the pancake thickness parameter. The relevant parameter for this is the mean distance of the electrons behind the shower front, $\langle h \rangle$, the mean pancake thickness parameter. In Fig. 8 this quantity is plotted for the set of showers at 10^{17} eV. Again the fluctuations are considerably larger for protons than for iron. In addition one can see that the mean pancake thickness parameter is almost independent of shower height and of shower type. Calculations for showers for 10^{18} eV give similar results.

In the present calculations $L = \langle h \rangle$ has been fixed for the full shower development. From Fig. 8 it can be seen that $L = 4.3$ m is a reasonable average value for iron-induced air showers, and $L = 3.9$ for proton-induced air showers. Where the width of the function at $1/e$ of the maximum can be shown to be approximately $1.5L$. The fluctuations in the average value of L are small with respect to the fluctuations in the shower profiles and not considered in further analysis.

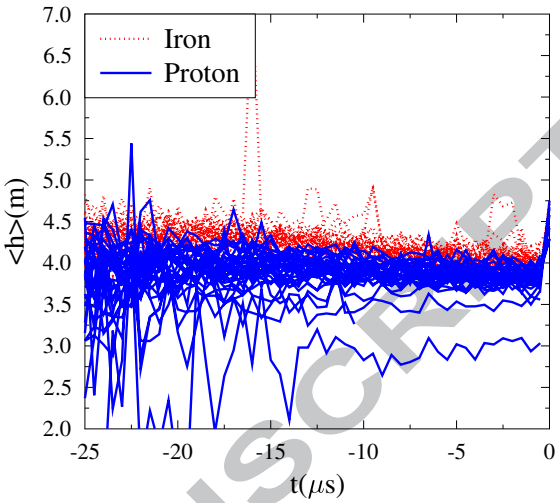

Figure 8: Mean distances of electrons behind the shower front for iron (red curves), and proton (blue curves) induced showers, as function of the negative shower time.

6. Composition

As a first application of the hybrid approach we study the LDF for proton- and iron-induced showers using MGMR in combination with CONEX-MC-GEO. The smoothed shower profiles extracted from each Monte-Carlo simulation are used in the calculation of the radio signal. For the calculation at short distances we use a suppression coefficient of $a = 100$, since in Section 3 it is shown that this value gives reliable results at the distances considered here. The maximum of the field strength as function of distance is shown in Fig. 9. This is done for an observer placed on the x-axis where the charge-excess and geo-magnetic fields interfere constructively. This figure shows that the slope for iron-induced showers is less steep than for protons. One also sees that at a distance of $d = 100$ m the calculated signal strength for iron and proton showers is almost the same. These features were also observed in REAS2 calculations [1].

To express the differences in the LDF more clearly we introduce a variable that is relatively easy to extract from data,

$$R^{25}_{50/300} = P(50, f > 25)/P(300, f > 25) \qquad (22)$$

where $P(d, f > 25)$ is the power in the pulse for frequencies larger than 25 MHz at a distance d m from the shower core. In Fig. 10 the results of the calculations are displayed in a histogram. The averages of the values for iron- and proton-induced showers differ strongly, however due to

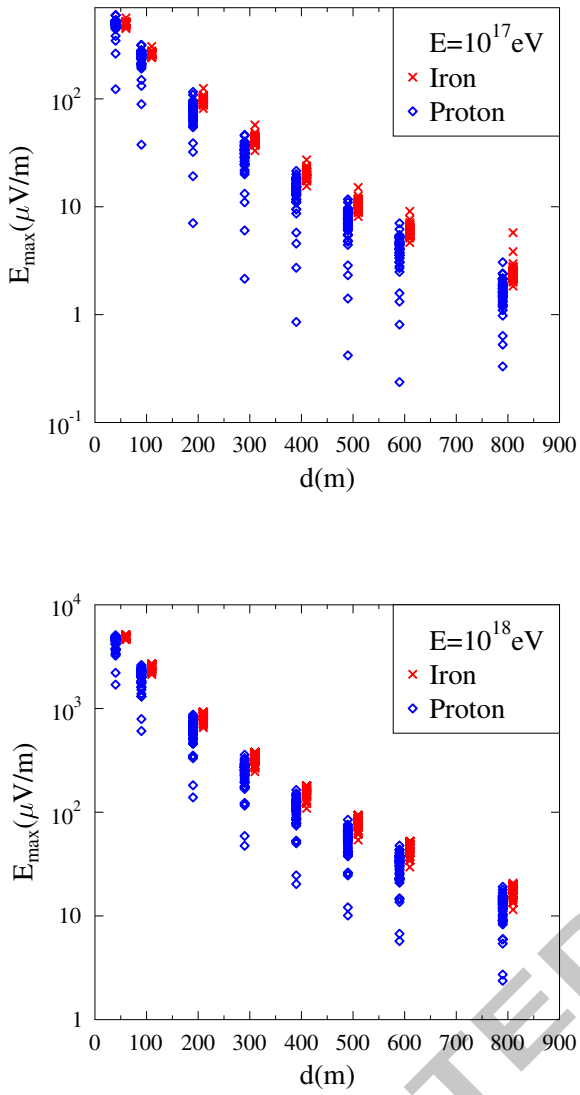

Figure 9: The LDFs are shown for proton (blue diamonds) and iron (red crosses) induced showers at an energy of 10^{17} eV (top), and 10^{18} eV (bottom), displayed in Fig. 6. The LDFs are given for an observer position leading to constructive interference between the charge excess contribution and the contribution due to geo-magnetic radiation.

shower-to-shower fluctuations some of the proton showers give rather similar values as for iron. The proton showers that give a similar value for $R^{25}_{50/300}$ are showers which have profiles (see Fig. 6) very similar to those of iron. At higher energies the average value of $R^{25}_{50/300}$ differs less between proton- and iron-induced showers. This is a direct consequence of the fact that X_{max}, the important parameter responsible for the observed effect, differs less for the different primary particles at higher energies, as can be seen in Fig. 9. As noted earlier the LDF, and thus also $R^{25}_{50/300}$, depends on the orientation of the observer with respect to the shower and comparisons should thus be made at the same azimuth with respect to the shower core. It has been checked that the qualitative differences between iron and protons remain as shown in Fig. 10 also for other azimuth positions of the observer. The reason for this is that the charge-excess fraction is similar for proton- and iron-induced showers.

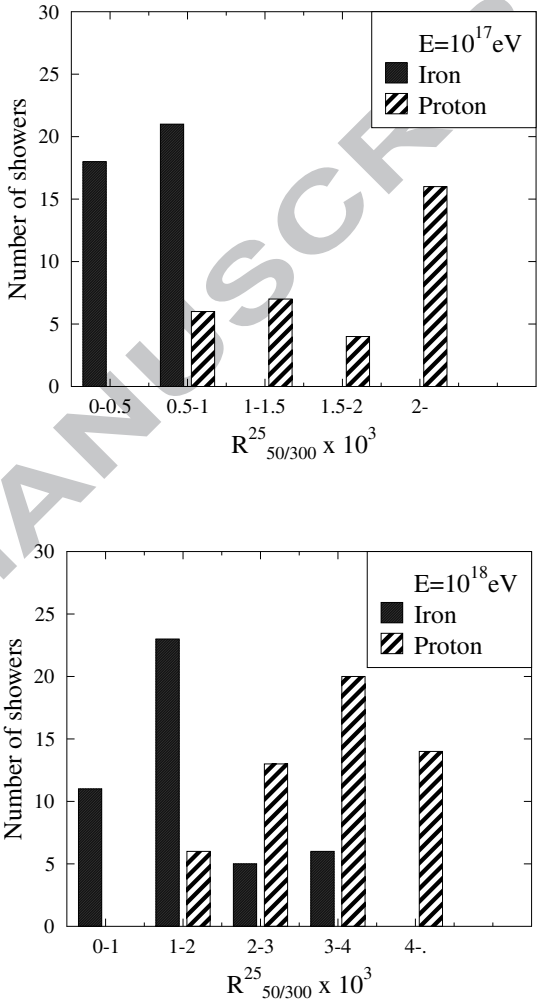

Figure 10: $R^{25}_{50/300}$, see text, for the 40 simulated proton and iron showers at an energy of $E = 10^{17}$ eV (top) and $E = 10^{18}$ eV (bottom).

7. Summary and Conclusions

We have derived a new expression for the electric field emitted by an EAS at close proximity to the shower axis in the MGMR model. It differs from the expression used for the pulse strength at large distances by a change of integration variables. This change of variables expresses

that at large distances the pulse shape is basically determined by the shower profile where the pancake thickness is integrated over. At short distances the picture is reversed and the pulse shape is determined by the pancake function and the shower profile can be integrated.

Due to the fact that the electron density is finite when the shower reaches Earth the pulse height becomes divergent at short distances from the core. This we have resolved by -artificially- suppressing the shower at small heights above the surface of the Earth. We show that this allows us to get accurate numerically-stable results at distances down to 30 m. At smaller distances other effects such as the lateral spread of the electrons in the shower, as well as shower-to-shower fluctuations will be important which are not included in the present schematic approach. In a future publication these effects will be considered in detail.

Since at short distances, the pulse shape is determined by the pancake function while at large distances it is governed by the shower profile this offers the possibility to use the LDF of the radio pulse to distinguish iron- and proton-induced showers. Before addressing this point we have added the radiation due to charge excess as the most important secondary process. It is shown that the determination of the polarization as a function of the azimuth angle can be used to study the different emission mechanisms of radio emission from an EAS. We show that the LDF is a very powerful tool to distinguish iron- and proton-induced showers although the effects of shower-to-shower fluctuations for protons can be large, where at the same time the power at a distance of 50 m from the shower core can be used as a measure for the energy.

8. Acknowledgment

This work is part of the research program of the 'Stichting voor Fundamenteel Onderzoek der Materie (FOM)', which is financially supported by the 'Nederlandse Organisatie voor Wetenschappelijk Onderzoek (NWO)'.

References

[1] T. Huege, R. Ulrich, R. Engel, Astropart. Phys. **30**, 96 (2008).
[2] Olaf Scholten, Klaus Werner, and Febdian Rusydi, Astropart. Phys. **29**, 94 (2008).
[3] Klaus Werner and Olaf Scholten, Astropart. Phys. **29**, 393 (2008)
[4] H. Falcke, et al., Nature **435**, 313 (2005).
[5] W.D. Apel, et al., Astropart. Physics **26**, 332 (2006).
[6] D. Ardouin, et al., Astropart. Physics **26**, 341 (2006).
[7] D. Ardouin and the CODALEMA Collaboration, Astropart.Phys., **31**, 192 (2009).
[8] H. Falcke and P. Gorham, Astropart. Phys. **19**, 477 (2003).
[9] D.A. Suprun, P.W. Gorham, J.L. Rosner, Astropart. Phys. **20**, 157 (2003).
[10] T. Huege, H. Falcke, Astronomy & Astrophysics **430**, 779 (2005)
[11] J.V. Jelley, et al., Nature **205**, 327 (1965).
[12] N.A. Porter, C.D. Long, B. McBreen, D.J.B Murnaghan and T.C. Weekes, Phys. Lett. **19**, 415 (1965).
[13] F.D. Kahn and I. Lerche, Proc. Royal Soc. London **A289**, 206 (1966).
[14] H.R. Allan, Prog. in Element. part. and Cos. Ray Phys. **10**, 171 (1971).
[15] A.M. van den Berg for the Pierre Auger Collaboration, Proc. of the 30th ICRC, Merida, Mexico **5**, 885 (2008)
[16] J. Coppens, Pierre Auger Coll., Nucl. Instr. and Meth. A **604**, S41 (2009).
[17] B. Revenu, Pierre Auger Coll., Nucl. Instr. and Meth. A **604**, S37 (2009)
[18] O. Scholten and K. Werner, Nucl. Instr. and Meth. A **604**, S24 (2009).
[19] T. Gousset, J. Lamblin, and S. Valcares, Astropart. Phys. **31**, 52 (2009).
[20] C. Riviere, Contribution nr. 52 to the ARENA 2010 conference, Nantes, to be published.
[21] V. Marin, Contribution nr. 64 to the ARENA 2010 conference, Nantes, to be published.
[22] M. Ludwig, and T. Huege, Contribution nr. 31 to the ARENA 2010 conference, Nantes, to be published.
[23] T. Huege, et al., Contribution nr. 34 to the ARENA 2010 conference, Nantes, to be published.
[24] J. Knapp et al., Astropart. Phys. **19**, 77 (2003)
[25] T. Huege, H. Falcke, Astronomy & Astrophysics **412**, 19 (2003).
[26] G. Agnetta et al., Astropart. Phys. **6**, 301 (2003)
[27] J.D. Jackson, Classical Electrodynamics, Wiley, New York, 1999.
[28] G.A. Askaryan, Sov. Phys. JETP **14**, 441 (1962); **21**, 658 (1965).
[29] G.N. Afanasiev, V.G. Kartavenko, and Yu.P. Stepanovsky, J. Phys. D **32**, 2029 (1999)
[30] W.D. Apel et al. -LOPES collaboration, Astropart. Phys. **32**, 294 (2010)
[31] G. Bossard, H.J. Drescher, N.N. Kalmykov, S. Ostapchenko, A.I. Pavlov, T. Pierog, E.A. Vishnevskaya, and K. Werner, Phys.Rev. **D63**, 054030 (2001)
[32] T. Bergmann, R. Engel, D. Heck, N.N. Kalmykov, Sergey Ostapchenko, T. Pierog, T. Thouw, K. Werner, Astropart.Phys. **26**, 420 (2007)